# Comparison of the thermal effects on LWIR optical designs utilizing different infrared optical materials

Jeremy Huddleston, Alan Symmons, Ray Pini
LightPath Technologies, Inc., 2603 Challenger Tech Ct, Ste 100, Orlando, FL, USA 32826

## ABSTRACT

The growing demand for lower cost infrared sensors and cameras has focused attention on the need for low cost optics for the long wave and mid-wave infrared region. The thermal properties of chalcogenides provide benefits for optical and optomechanical designers for the athermalization of lens assemblies as compared to Germanium, Zinc Selenide and other more common infrared materials. This investigation reviews typical infrared materials' thermal performance and the effects of temperature on the optical performance of lens systems manufactured from various optical materials.

**Keywords:** Precision glass molding, long wave infrared, LWIR, thermal camera, athermal, athermalization, chalcogenide, SWaP-C.

## 1. INTRODUCTION

Over the past ten years, the prices for thermal imaging sensors have decreased dramatically. The resulting cost savings has significantly increased the quantities of thermal imagers sold. However, the high cost of traditional materials for thermal lenses has become the limiting factor in overall camera costs. Optics manufacturers are looking for high volume, low cost methods to produce infrared optical systems. The technological roadmap for infrared optical systems is following the same path that visible camera systems have followed in the recent past; from large SLR type cameras to small handheld cameras and finally to cell phone camera systems. The enabling technology for the visible region was molding of optical lenses. The advantages of molded optics apply even more so to the LWIR region, where the potential for cost reduction relative to existing lens technologies is even greater.[1] Specifically, the chalcogenide moldable materials for IR have improved thermal properties relative to traditional IR materials, such as Germanium.[2] These athermal characteristics are extremely valuable in reducing the cost, size and complexity of mechanical compensation techniques required for less athermal materials. Furthermore, the availability of different commercial chemical compositions of the chalcogenides enable potential trade offs on optical and mechanical characteristics. The focus of this study is to explore the potential performance benefits of these moldable materials, and additionally to improve upon the thermal analysis techniques used to evaluate the expected thermal effects on system performance for low-cost optics.

## 2. ATHERMAL DESIGN THEORY

### 2.1 Theory Introduction

There are three main ways to combat the effects of temperature in an optical system: active mechanical compensation (electromechanical), passive mechanical compensation (optomechanical), and passive optical compensation (material).[3] Each successive method represents reduced cost, size and complexity. Most lenses may be mechanically compensated to some degree, so in order to reduce system size and cost, the lens material properties must provide most or all of the compensation. Therefore, we will address the effects of passive optical athermalization in the absence of mechanical compensation, by comparing the properties of various lens materials.

Ideally, an "athermal" or "athermalized" lens would have no change to image quality over the full operating temperature range across the full FOV of any detector with which it is used. In practice, there are many limitations to this ideal for which a lens user or purchaser should be aware.

Infrared Technology and Applications XL, edited by Bjørn F. Andresen, Gabor F. Fulop, Charles M. Hanson, Paul R. Norton, Proc. of SPIE Vol. 9070, 90702E · © 2014 SPIE
CCC code: 0277-786X/14/$18 · doi: 10.1117/12.2050686

The first issue is that there is no agreed-upon quantitative definition for an athermal lens, such that lens providers may choose to call any lens "athermal" without specifying the actual lens performance over temperature[4]. The athermal characteristics of a lens system may be evaluated in various ways, ranging from theoretical approximations ("rules of thumb" analytical formulas) to predictive modeling of expected performance through rigorous optomechanical design of the lens, housing and detector components. In some cases, the use of the term "athermal" simply describes a decrease in thermal sensitivity relative to other lenses. Such a lens may also be described as having "material athermalization", meaning that the natural thermal properties of the lens material make it *relatively* insensitive to temperature compared to traditional materials and existing lenses on the market. This leaves much ambiguity as to the actual level of athermal performance that one should expect when using the lens.

Another limitation is that ideal athermalization techniques are often complex and expensive. With growing industry pressure to reduce the cost and size of lens systems, many of these theoretical methods for athermalization have become less practical or affordable. Optically passive techniques require multiple elements with varying materials, which increase cost and size. Mechanically (or optomechanically) passive techniques require multiple materials in the lens or camera housing which may also increase the cost and size of overall camera system. Thus, a trade-off must be found between an ideal solution for perfecting image quality over temperature, and achieving a small, low-cost camera system.

Further limitations arise from the incomplete use of optical theory to implement athermalization. Early efforts in deriving formulas for athermal solutions relied on many approximations and assumptions in the underlying optical theory (ex. paraxial optics, thin lenses, no aberrations, ideal housings, etc).[3,5,6,7] These approximations are often misunderstood, and the assumptions are often unrealistic when applied to practical design problems. The impact can be even more problematic when trade-offs of performance and material selection are necessary for achieving aggressive goals of cost and size. For instance, small focal lengths, low F numbers, large FOVs, ray aberrations, housing constraints, and detector design can all lead to reduced validity of the theoretical formulations. The aforementioned lack of an athermal image quality standard has enabled these approximations to persist in literature and replace a more a rigorous methodology for athermalization analysis. [1,3,4,8,9,10]

The scope of this study is to begin with the well-known analytical approximations, and then compare to more realistic expectations from modeling of practical systems. This will form the proper foundation for comparing a select group of available IR lens materials to reveal advantages that can be utilized for achieving realistic design goals.

### 2.2 Predictions of Analytical Theory

Athermalization theory has been well documented and has been used for athermalized lens designs, often without addressing the applicability of the underlying assumptions. Since we wish to establish a baseline relative to broadly used theory, we will review this theory first without addressing the weaknesses of these assumptions, and later compare to modeled results.

We start by noting that the change in focus $\Delta f$ with temperature $\Delta T$ of an ideal lens of nominal focal length $f_o$ may be calculated by the use of a thermal glass constant $\gamma_T$ related to the refractive index $n$, the temperature coefficient of refractive index dn/dT, and the coefficient of thermal expansion (CTE) of the lens material $\alpha_L$ as follows: [4,8,10]

$$\Delta f = -\gamma_T \cdot f_o \cdot \Delta T \tag{1}$$

where

$$\gamma_T = \left(\frac{1}{n-1}\right) \cdot \frac{dn}{dT} - \alpha_L \tag{2}$$

This only addresses the lens, so we can add a housing CTE $\alpha_H$ to equation (1) to obtain a combined thermal constant $\beta_T$,

$$\beta_T = \gamma_T + \alpha_H \tag{3}$$

where the thermal focal shift now becomes

$$\Delta f = -\beta_T \cdot f_o \cdot \Delta T \tag{4}$$

This treatment assumes that the housing mounts to the lens at the principal plane and mounts to the detector at the image plane, as shown in Figure 2 below.

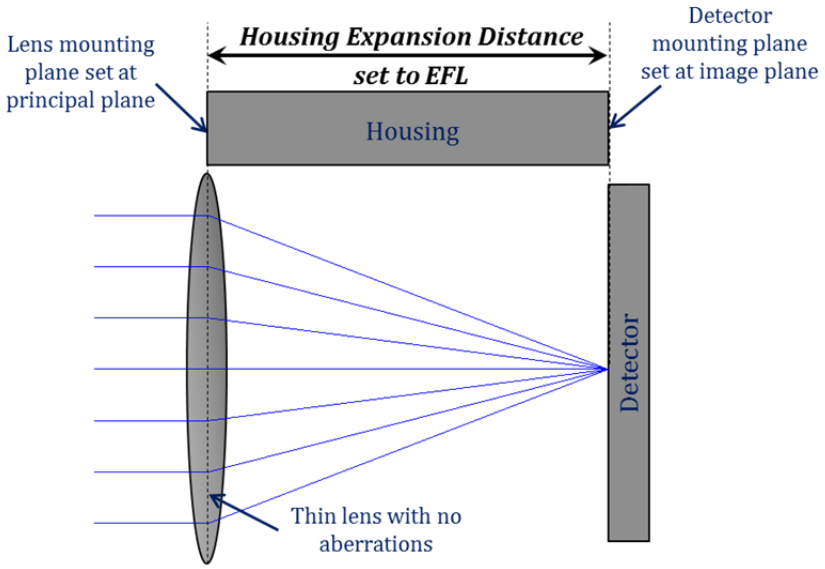


***Figure 1 – Simplified optomechanical assumptions of equation (4) from approximate athermalization theory.***

This is an erroneous assumption in most cases, but if we temporarily accept it, we find that the change in focus is proportional to the sum of the housing CTE and the thermal glass constant. The thermal properties referenced above for a few conventional IR materials and several formulations of chalcogenides are found in Table 1, with the assumption of an Al housing. Although the chalcogenide materials selected may be obtained under various trade and brand names, we will refer to them by their chemical composition to avoid confusion.

**Table 1**: Optical/thermal properties of several LWIR lens materials

| **Property** | **Symbol** | **Unit** | **Ge**[1] | **ZnSe**[2] | **ZnS**[3] | **$Ge_{10}As_{40}Se_{50}$**[4] | **$Ge_{28}Sb_{12}Se_{60}$**[4] | **$As_{40}Se_{60}$**[4] |
|---|---|---|---|---|---|---|---|---|
| Index at 10.6μm | n | N/A | 4.003 | 2.403 | 2.192 | 2.609 | 2.600 | 2.778 |
| Thermal Coef. of Refractive Index | dn/dT | $10^{-6}$/°C | 400 | 61 | 43 | 20 | 70 | 32 |
| Lens CTE | $\alpha_L$ | $10^{-6}$/°C | 5.9 | 7.1 | 6.6 | 20.4 | 14.5 | 20.8 |
| Thermal Glass Constant | $\gamma_T$ | $10^{-6}$/°C | 127 | 36 | 29 | -8 | 29 | -3 |
| Housing CTE (Al) | $\alpha_H$ | $10^{-6}$/°C | 23.6 | 23.6 | 23.6 | 23.6 | 23.6 | 23.6 |
| Combined Thermal Constant | $\beta_T$ | $10^{-6}$/°C | 151 | 60 | 53 | 16 | 53 | 21 |

[1] *http://eom.umicore.com/en/infrared-optics/blanks/germanium-datasheet.pdf*
[2] *http://www.crystran.co.uk/userfiles/files/zinc-selenide-znse-data-sheet.pdf*
[3] *http://www.crystran.co.uk/userfiles/files/zinc-sulphide-flir-zns-data-sheet.pdf*
[4] *LightPath Technologies, measured at 10.6μm wavelength*

The thermal focal shift we have described is only meaningful when applied to a relevant criterion for acceptable focal shift that keeps the lens "athermal". As previously mentioned, there are no well-established performance criteria, so many have chosen to use the "diffraction limited depth of focus" $DOF_{DL}$ of the lens, which is a theoretical value derived by further approximations to be: [4,8,10]

$$DOF_{DL} = \pm 2 \cdot \lambda \cdot (F/\#)^2 \tag{5}$$

By this definition, the lens is "athermal" if the thermal focal shift is less than the paraxial depth of focus. For example, an F/1.3 lens operating at a center wavelength of 10μm would have a theoretical depth of focus of ±34μm, so any

thermal focal shift less than 34μm would be considered athermal. Since the thermal focal shift in equation (4) is dependent on the temperature change, we can combine equations (4) and (5) to find a full temperature range $T_A$ over which the lens is considered to be "athermal", as follows:

$$T_A = 2 \cdot \Delta T = \frac{4 \cdot \lambda \cdot (F/\#)^2}{-(\gamma_T + a_H) \cdot f_o} \quad (6)$$

Table 2 shows athermal temperature ranges for the materials in Table 1 across typical focal lengths and F numbers. Values greater than 125°C indicate theoretical athermalization from -40°C to +85°C, while values greater than 80°C would satisfy less demanding applications that require only -20°C to +60°C athermalization. Germanium can be seen to have the worst thermal performance of all of the materials considered, and would not be considered athermal across most of the considered ranges of EFL and F/#. ZnSe and ZnS could be considered athermal only for low EFLs, while two of the chalcogenide compositions extend theoretical athermalization to a larger range of lenses. As mentioned earlier, any of these materials could be applied to an athermal lens system by introducing mechanical compensation. However, the more athermal the material, the less mechanical compensation is needed, and thus the lower the cost, size and complexity of the entire camera system.

**Table 2: Comparison of temperature ranges in °C over which a lens would be theoretically athermal. Green: >125°C (-40 to +85°C); Yellow > 80°C (-20 to +60°C); Orange <80°C (not athermal)**

| F/# | EFL | Ge | ZnSe | ZnS | $Ge_{10}As_{40}Se_{50}$ | $Ge_{28}Sb_{12}Se_{60}$ | $As_{40}Se_{60}$ |
|---|---|---|---|---|---|---|---|
| 1.0 | 5 | 53 | 133 | 151 | 514 | 151 | 383 |
| | 10 | 27 | 67 | 75 | 257 | 76 | 191 |
| | 20 | 13 | 33 | 38 | 128 | 38 | 96 |
| | 50 | 5 | 13 | 15 | 51 | 15 | 38 |
| 1.3 | 5 | 90 | 225 | 255 | 868 | 256 | 647 |
| | 10 | 45 | 113 | 127 | 434 | 128 | 323 |
| | 20 | 22 | 56 | 64 | 217 | 64 | 162 |
| | 50 | 9 | 23 | 25 | 87 | 26 | 65 |

*Note: Assumes Al housing (CTE = 23.6 x $10^{-6}$/°C) and 10μm wavelength*

While the values in Table 2 highlight the potential of chalcogenide materials in general, they also reveal that not all chalcogenides exhibit the same thermal advantages due to their differing chemical compositions. For instance, the $Ge_{10}As_{40}Se_{50}$ and $As_{40}Se_{60}$ compositions exhibit significantly better thermal properties relative to Ge, ZnSe and ZnS, while the $Ge_{28}Sb_{12}Se_{60}$ composition only has a significant advantage compared to Ge. Fortunately, there are a many chalcogenide compositions available, and some that are still under investigation, covering a large range of optical properties from which to choose. [1, 11,12] . While this makes it hard to draw conclusions about all chalcogenides, it provides the needed leverage for chalcogenide lens manufacturers to choose the best material to achieve the right balance of performance and cost for each specific application. Additionally, chalcogenides offer other advantages not seen in Table 2, such as lower wavelength dispersion than ZnSe and ZnS, as well as lower cost and more consistent availability of raw material. These other differences indirectly manifest as thermal performance advantages when taken as a whole for net system performance, as will be shown in the following sections.

## 3. OPTICAL MODELING METHODOLOGY

### 3.1 Modeling Introduction

The analytical treatment in the previous section is well-known and commonly used, but is based on many approximations and assumptions, such as paraxial optics, thin lenses, no aberrations, no field curvature, no dispersion, ideal housing mechanics, etc. While the results this theory are often used to draw conclusions about athermalization, a more thorough treatment is needed to either refine or validate these assumptions. Rather than address the merits of each assumption individually – a lengthy exercise that would still neglect interactive effects – we can instead use optical modeling of thermal performance with realistic design constraints. Table 3 outlines an example set of specifications for an LWIR lens design. Although this table does not represent any one single set of requirements from camera manufacturers, it is a representative example showing the many optical parameters that must be balanced during optimization and analysis. In reality, each camera manufacturer often has additional unique lens requirements beyond those listed, such as dimensional limitations for optomechanical integration, but these will serve as the most basic set of requirements common to most applications. All of the factors in Table 3 except EFL and F/# are absent from the theoretical methods described in the previous section. Taken as a whole, these specifications can limit even the nominal performance of a realistic lens design and thus affect the resulting performance over temperature.

**Table 3: Example specifications for a low cost thermal imaging lens showing typical requirements that must be balanced for optimal performance, cost, size and manufacturability.**

| Parameter | | Notes | Typical Specification |
|---|---|---|---|
| Detector resolution / pitch | | Typical low-cost LWIR camera(FLIR Quark, DRS Tamarisk, L3 Nanocore) | 320x240 / 17μm |
| FPA cover window | | Standard Si substrate thickness – varies by detector | 0.7mm |
| Wavelength Weightings | | Unique to the spectral sensitivity of each detector | Gaussian (8-12μm) |
| Number of lens elements | | Cost requirements drive toward singlet designs when possible | 1-2 |
| Optical Track Length | | Front lens apex to image plane | <25mm |
| Transmission | | Affected by material absorption and coating efficiency, as well as diffraction efficiency for hybrid lenses; lower transmission may be compensated for by lower F/# | >90% |
| EFL | | Driven by FOV and F/# requirements | 8mm |
| F/# | | Affects both brightness and diffraction-limited MTF | 1.3 |
| HFOV | | Can be derived from EFL and distortion for a given sensor | 40deg |
| MTF (Min S/T @ 29.4cyc/mm) | On-axis | Min Sag/Tan MTF at image center | >45% |
| | VFOV | Min Sag/Tan MTF at ±Vertical FOV | >35% |
| | HFOV | Min Sag/Tan MTF at ±Horizontal FOV | >25% |
| | Corner | Min Sag/Tan MTF at image corners | >15% |
| Distortion | | At image corner relative to center – typically increases with FOV | <10% |
| Relative illumination | | At image corner relative to center – typically decreases with FOV | >85% |
| Flare | | Geometric radius of spot size across the field. Large flare can manifest as stray light or ghosting, and adds to background noise | <170μm (10 pixels) |

### 3.2 Detector Considerations

The first few parameters in Table 3 are related to the detector with which the lens will be used. Although lenses are typically advertised independent of the detector in order to be sold to multiple camera makers, the best optical designs will be those whose performance has been tailored to a particular detector and application. For example, a lens designed without taking the cover window into account will have slightly different performance when a cover window of sufficient thickness and refractive index is used. A small MTF shift is introduced due to field curvature changes that are affected by the differing path lengths of each field propagating through the cover window. Similarly, variations in performance may come from the spectral ranges and sensitivities of different detectors. Figure 2 shows an overlay of MTF vs. field plots for the same lens design using 2 different detectors. Both cases have been adjusted for best focus, but each has different spectral weightings and cover window thickness.

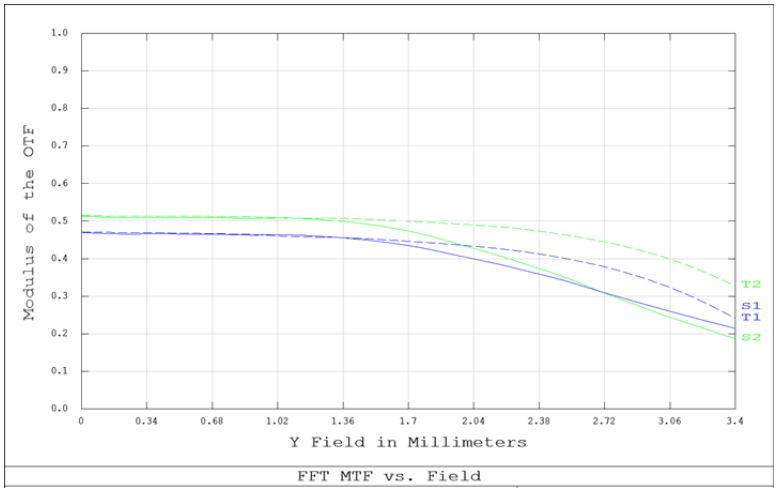


***Figure 2 –*** *MTF vs. Field overlay for the same lens design used with 2 detectors with different cover window thickness and spectral sensitivity.*

### 3.3 Optical Considerations

The remaining factors in Table 2 relate to the optical parameters of the system that each contribute to a different aspect of image quality and performance. These lead to a complex combination of possible designs with varying performance across all parameters. For multi-element designs with different material combinations, much of the variation in performance is often due to the large number of possible design forms rather than isolated material effects. While many have attempted to compare multi-element designs with different materials, most of these optical parameters, such as distortion and relative illumination, are not reported and may not stay constant across designs.

In order to minimize the effects of differing design styles and optimization techniques, we will consider a singlet lens for comparing material effects alone. All designs will have the same basic design form that minimizes the size and cost of the lens system. Although this removes the ability to evaluate combinations of lens materials, it is an important starting point to determine whether or not theory matches practical designs, even for the simplest case of a singlet. Additionally, such a comparison is valuable in representing the lowest cost and smallest form factor solution that may be achieved for the given specification.

## 4. MODELING RESULTS AND ANALYSIS

### 4.1 Introduction to Results

Each of the materials from Tables 1 and 2 were used to create a singlet design optimized to meet the example specifications outlined in Table 3. The design form was chosen to be the same for each: a concave meniscus with a front aperture stop that would enable the shortest optical track length while maximizing the performance across the image. Realistic manufacturing constraints were applied, which may differ across the designs due to the limitations of fabrication methods used for each respective material, such as slopes and curvatures. Optomechanical integration constraints were also considered.

### 4.2 Nominal Design Comparison

Table 4 shows the results of designing a singlet to the specifications of Table 3 across all of the materials outlined in Tables 1 and 2. Several of the material parameters from Table 1 are repeated for reference, along with the addition of the Abbe number $A_T$ of the thermal band, which is given by:

$$A_T = \frac{n_{10}-1}{n_8-n_{12}} \tag{7}$$

where $n_i$ is the index at wavelength i. The Abbe number is inversely proportional to the dispersion, such that lower Abbe numbers indicate a higher sensitivity to wavelength and larger performance shift over the full LWIR band. High dispersion materials often require at least one surface to be a hybrid diffractive/refractive surface, as diffractives have an opposite dispersion relative to refractives, and therefore serve to partially compensate for wavelength sensitivity.

**Table 4: Nominal design performance matrix for singlets of various lens materials.**

| Parameter | | Spec | Design 1 | Design 2 | Design 3 | Design 4 | Design 5 | Design 6 | Unit |
|---|---|---|---|---|---|---|---|---|---|
| Glass Composition | | | Ge | ZnSe | ZnS | $Ge_{10}As_{40}Se_{50}$ | $Ge_{28}Sb_{12}Se_{60}$ | $As_{40}Se_{60}$ | |
| Material Index (at 10.6µm) | | | 4.003 | 2.403 | 2.192 | 2.609 | 2.6032 | 2.7782 | |
| dn/dT x10-6/°C (at 10.6µm) | | | 400 | 61 | 43 | 20 | 70 | 32 | $10^{-6}$/°C |
| Thermal Abbe (8-12µm) | | | 865 | 58 | 23 | 172 | 109 | 160 | |
| Hybrid diffractive/refractive | | | No | Yes | Yes | Yes | Yes | Yes | |
| F/# | | 1.3 | 1.3 | 1.3 | 1.3 | 1.3 | 1.3 | 1.3 | |
| Horizontal FOV | | 40 | 40 | 40 | 40 | 40 | 40 | 40 | Deg |
| EFL | | ~8 | 7.8 | 7.9 | 7.9 | 7.9 | 7.9 | 7.9 | mm |
| Relative Illumination | | >85 | 92 | 89 | 90 | 92 | 92 | 93 | % |
| Distortion | | <10 | 9 | 8 | 7 | 8 | 8 | 8 | % |
| MTF (Min S/T @ 29.4cyc/mm) | On-axis | >45 | 50 | 49 | 47 | 50 | 50 | 50 | % |
| | VFOV | >35 | 43 | 41 | 35 | 46 | 47 | 49 | % |
| | HFOV | >25 | 35 | 31 | 21 | 37 | 37 | 39 | % |
| | Corner | >15 | 22 | 17 | 9 | 25 | 25 | 25 | % |
| Flare (Geometric Radius) | | <170 | 170 | 172 | 174 | 170 | 125 | 142 | µm |
| Optical Track Length | | <25 | 22.8 | 18.9 | 19.9 | 21.5 | 21.3 | 19.8 | mm |

It is apparent from Table 4 that some of the materials are better suited to achieve the nominal design requirements from Table 3 than others. For instance, the low index of ZnS combined with its high dispersion (low Abbe) limit the nominal MTF, even for unconstrained distortion and relative illumination.

We see from Design 1 that Ge enables an all-refractive solution, while all of the other materials have higher dispersions that require a diffractive compensator. ZnS has the highest dispersion and lowest refractive index, which lowers the nominal MTF that is achievable even with a diffractive compensator. Although ZnS showed potential for athermalization in Table 2, it would have a much lower margin for MTF drop over temperature than the other materials. Similarly, ZnSe shows some drop in nominal MTF for off-axis fields. The chalcogenide materials (designs 4-6) all show the best nominal performance due to their balance of relatively high index and moderate dispersion that is adequately compensated by a diffractive.

### 4.3 MTF-Based Depth of Focus

Equation (5) defined a diffraction limited depth of focus based on paraxial optics approximations. This method established a theoretical value for an acceptable focal shift to be ±34µm (68µm DOF) for an F/1.3 lens used at a center wavelength of 10µm for the LWIR band. However, this treatment neglects the actual MTF requirements for real world applications across the operating temperature range. A more thorough treatment would also take into account the effect of manufacturing tolerances, but since each lens manufacturer will be capable of hitting different tolerances, we will simply demonstrate the methodology by addressing temperature affects that are based on the material properties alone. As such, we will consider the depth of focus over which the MTF specifications of Table 3 are met. We start by examining the MTF through-focus curves against the performance criteria at each field point. Figure 3 demonstrates this for the on-axis field point of Design 1 from Table 4.

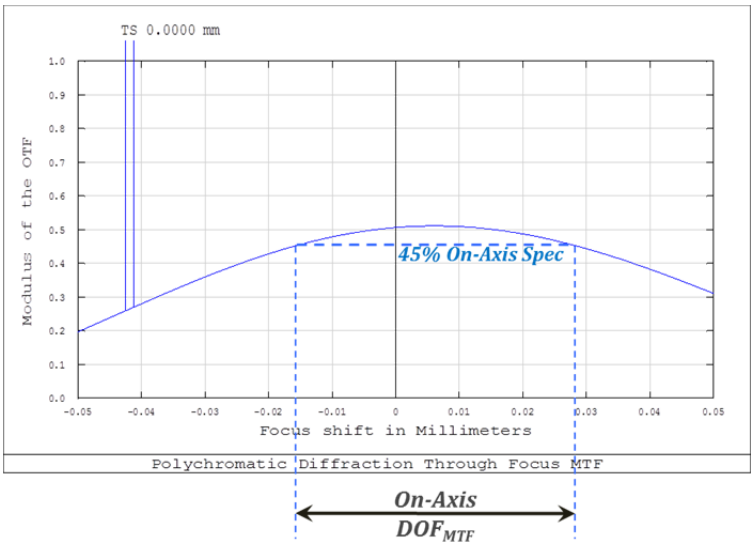


***Figure 3 – On-axis MTF through focus curve showing MTF-based depth of focus.***

As seen in Figure 3, the on-axis depth of focus is 44µm (-16µm to +28µm) against the 45% spec. This is much less than the 68µm depth of focus derived from the athermalization theory previously discussed. Furthermore, if the design is to be athermal across the entire image, we must consider the depth of focus based on all of the field points. Figure 4 shows the effect of evaluating all field points against the MTF specifications, which drops the MTF-based DOF down to 25µm.

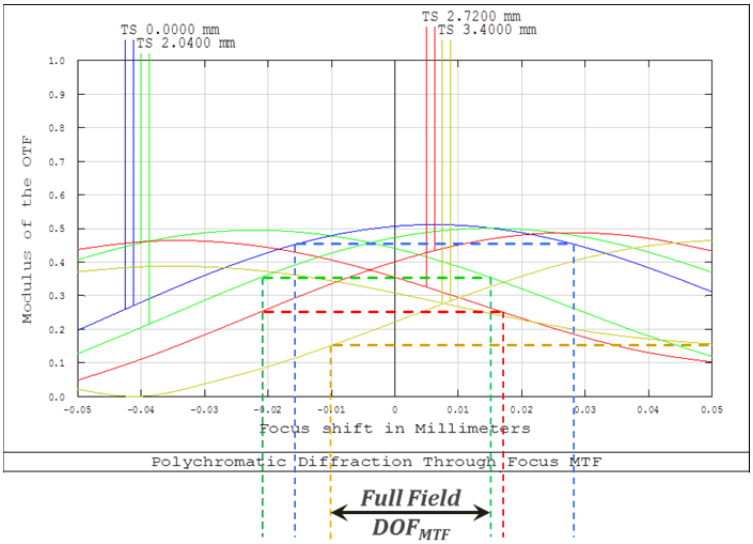


***Figure 4 – MTF through focus curves showing the full field MTF-based depth of focus.***

It is clear that the MTF-based depth of focus is significantly limited by the off-axis fields, especially by the alignment of the through-focus MTF curves of each field point. This misalignment is primarily due to field curvature and is a consequence of the trade-offs necessary in design. Field curvature can often be improved in multi-element lens systems, but would increase the overall size and cost of the imager. Even for doublet and triplet designs, however, there is typically some misalignment and asymmetry in the MTF through-focus curves that leads to decreased depth of focus across the entire field. This is true even for supposed "diffraction limited" lenses. This is because the diffraction limited criteria is applied from paraxial approximations, rather than the actual MTF *which is always less than the diffraction-limited MTF*.

Using the method shown in Figure 4, we can determine an MTF-based depth of focus for each lens design from Table 4. While this DOF is based on the previously established spec, we may also define an athermal DOF as a range over which there is a *relative* change in MTF performance, such as a 5-10% MTF drop from nominal across the field. The reason for these separate criteria is that some customers may be interested in meeting a minimum performance set by a fixed MTF specification, while others may be more concerned with the change in performance over temperature, regardless of how low the MTF is at the nominal temperature. While the former is more often the case, the latter is included for completeness. This will also highlight that the results of an athermalization analysis are highly dependent on the chosen criteria, even when based on MTF performance. Table 5 shows these different methods of determining the DOF.

**Table 5: Depth of focus in µm for each design based on the nominal MTF through-focus curves**
**Green: >125°C (-40 to +85°C); Yellow > 80°C (-20 to +60°C); Orange <80°C (not athermal)**

| **Depth of Focus** ***Method*** | **Design 1** Ge | **Design 2** ZnSe | **Design 3** ZnS | **Design 4** $Ge_{10}As_{40}Se_{50}$ | **Design 5** $Ge_{28}Sb_{12}Se_{60}$ | **Design 6** $As_{40}Se_{60}$ |
|---|---|---|---|---|---|---|
| Theoretical DOF (7.9µm EFL, F/1.3) | 68 | 68 | 68 | 68 | 68 | 68 |
| MTF-based DOF against MTF Spec | 25 | 10 | 0 | 28 | 28 | 27 |
| MTF-based DOF against 5% Drop | 17 | 20 | 22 | 16 | 20 | 18 |
| MTF-based DOF against 10% Drop | 32 | 36 | 41 | 30 | 36 | 32 |

If we assume that the thermal focal shift derived by paraxial theory in equations (1) through (4) is still correct (assumptions which will be addressed in the following section), then we can go on to substitute the MTF-based depth of focus $DOF_{MTF}$ into equation (4) to obtain an MTF-based athermal temperature range $T_{MTF}$ similar to theoretical one derived in equation (6), as follows:

$$T_{MTF} = \frac{DOF_{MTF}}{-(\gamma_T + \alpha_H) \cdot f_o} \quad (8)$$

Table 6 shows the resulting athermal temperature ranges obtained by different methods and criteria. We can see that MTF-based methods result in athermal temperature ranges that are very small for all of the crystalline materials. However, 2 of the 3 chalcogenide materials are athermal over a much larger temperature range, often exceeding the stringent -40°C to +85°C operating range. Even the lowest-performing chalcogenide material, $Ge_{28}Sb_{12}Se_{60}$, has a much larger athermal temperature range than Ge, ZnSe and ZnS, when evaluated against the MTF spec, and comes close to meeting the target -20°C to +60°C operating temperature range. Based on cost and manufacturability compromises, even $Ge_{28}Sb_{12}Se_{60}$ is likely to be acceptable with no mechanical athermalization for many applications.

**Table 6: Athermal temperature ranges in °C, from nominal MTF depth of focus.**
**Green: >125°C (-40 to +85°C); Yellow > 80°C (-20 to +60°C); Orange <80°C (not athermal)**

| Athermal Temperature Range | | ***Design 1*** Ge | ***Design 2*** ZnSe | ***Design 3*** ZnS | ***Design 4*** $Ge_{10}As_{40}Se_{50}$ | ***Design 5*** $Ge_{28}Sb_{12}Se_{60}$ | ***Design 6*** $As_{40}Se_{60}$ |
|---|---|---|---|---|---|---|---|
| ***Method*** | ***Specification*** | | | | | | |
| Approximate Analytical Theory | Theoretical Diffraction Limit | 57 | 143 | 161 | 550 | 166 | 409 |
| Theoretical focal shift with MTF-based DOF | Design Spec Limit | 21 | 21 | 0 | 228 | 69 | 163 |
| | 5% Relative Drop | 14 | 42 | 52 | 130 | 49 | 109 |
| | 10% Relative Drop | 27 | 76 | 98 | 244 | 86 | 194 |

### 4.4 Realistic optomechanical integration

The previous section corrected the theoretical depth of focus assumptions with realistic MTF-based values. However, the assumptions for the thermal focal shift of equations (1) through (4) were maintained, and will now be investigated.

The first assumption we will address is the use of the thin-lens approximation for deriving the relationship between the lens CTE and dn/dT expressed in the thermal glass constant. While this treatment captures the effects of changes in lens curvature and refraction at the lens surface, it neglects both the center thickness of the lenses as well as the finite sag of each surface. For very large EFLs with multiple elements, it is possible that the lenses may be thin enough relative to the EFL for this approximation to be valid. However, smaller imagers often have lenses whose finite thicknesses make up a considerable percentage of the optical track length and EFL.

The next problem is that the housing CTE is incorporated with the assumption that it is mounted to the principal plane of the lens system. In reality, the best mounting position is often on the front or back flange of the lens, rather than at the principal plane. In some cases, the principal plane is far from the mounting positions. One may assume that principal plane is at the mid-point between the lens surfaces, making a mount to both flanges an appropriate approximation, but we will see later that this is also an invalid assumption for the designs we have considered.

Finally, the distance of the housing to the detector is often approximated by the distance to the image plane. In reality, the mechanics of the detector often necessitate a mounting location significantly offset along the optic axis from the image plane. Furthermore, there may be different material CTEs within the detector for mounting the detector FPA to the mounting plane of the housing.

Figure 5 shows a simple optomechanical layout for lens Design 1. The principal plane and EFL are shown, and you can see that due to the strong meniscus lens form, the EFL is less than half of the actual distance over which the housing will expand. Thus, the thermal expansion of the housing will cover more than twice the distance accounted for by the EFL used in the theoretical approximations! In addition, the base of the detector has a non-aluminum CTE that will expand at a different rate from the detector mounting plane back up to the image plane.

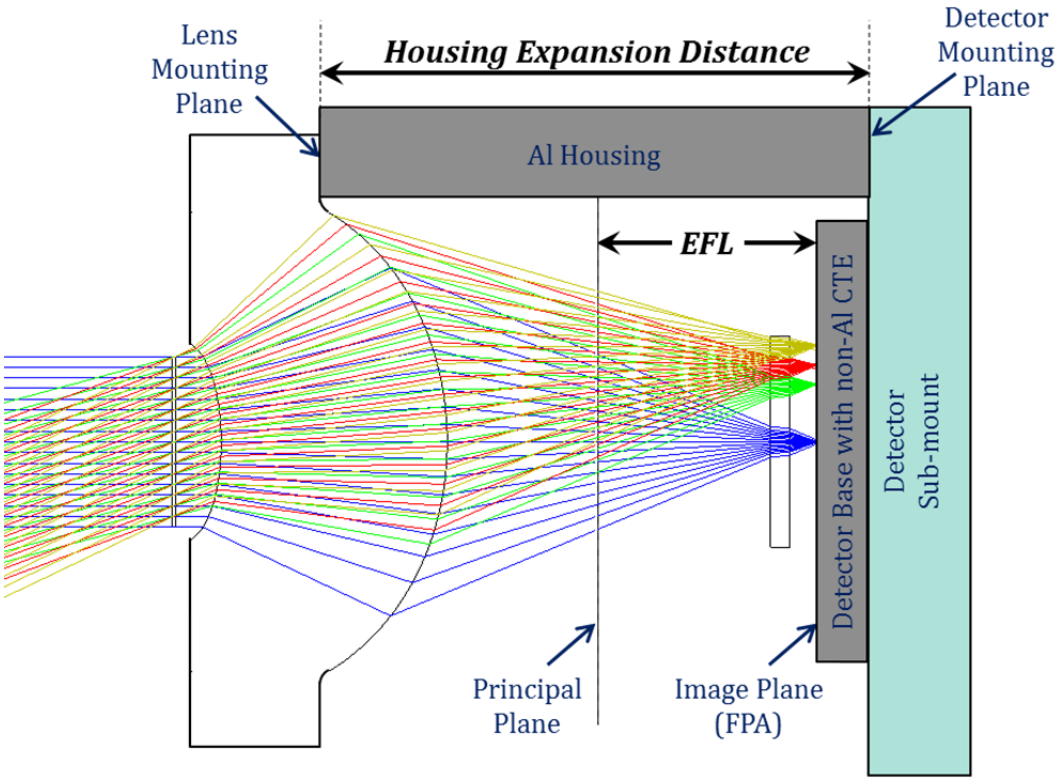


***Figure 5 – Optomechanical layout for lens design 1 showing that the EFL is a poor approximation for the housing distance from the lens flange to the detector mount.***

A thorough thermal analysis was done on each of the designs presented earlier, which included the actual effects of the factors noted above. Thick lens expansion, flange locations and mounting points to the housing were all considered. The range over which the actual MTF specifications were met for the optomechanical model was determined for each design. This method provided a more direct and accurate way to evaluate athermalization compared to the approaches discussed in the previous sections. Table 7 shows the athermalized temperature range for the six designs based on the more rigorous optomechanical thermal analysis, along with all of the analysis methods previously presented.

**Table 7: Athermal temperature ranges in °C, from optomechanical analysis with MTF-based criteria. (Shading shows relative athermalization only.)**

| Athermal Temperature Range | | ***Design 1*** Ge | ***Design 2*** ZnSe | ***Design 3*** ZnS | ***Design 4*** $Ge_{10}As_{40}Se_{50}$ | ***Design 5*** $Ge_{28}Sb_{12}Se_{60}$ | ***Design 6*** $As_{40}Se_{60}$ |
|---|---|---|---|---|---|---|---|
| ***Method*** | ***Specification*** | | | | | | |
| Approximate Analytical Theory | Theoretical Diffraction Limit | 57 | 143 | 161 | 550 | 166 | 409 |
| Theoretical focal shift with MTF-based DOF | Design Spec Limit | 21 | 21 | 0 | 228 | 69 | 163 |
| | 5% Relative Drop | 14 | 42 | 52 | 130 | 49 | 109 |
| | 10% Relative Drop | 27 | 76 | 98 | 244 | 86 | 194 |
| Optomechanical Focal Shift with MTF Analysis | Design Spec Limit | 7 | 9 | 0 | 79 | 31 | 61 |
| | 5% Relative Drop | 4 | 20 | 30 | 43 | 22 | 40 |
| | 10% Relative Drop | 9 | 38 | 59 | 88 | 38 | 73 |

## 5. CONCLUSIONS

We have compared several methods of athermal analysis and seen that the most realistic gauge of lens athermalization is based on modeling of optomechanical focal shift along with MTF criteria. This method invalidates many conclusions previously drawn by simplistic athermalization theory relying on often erroneous assumptions and approximations. Even for this method, however, a consistent criterion must be chosen, as seen by the large difference between specs that are based on absolute MTF limits vs. relative drops in MTF. Therefore, any evaluation of lens athermalization must take the lens design, optomechanics and end application criteria into account.

Having established a thorough and realistic athermal analysis methodology, it has been shown that none of the materials considered can always be considered athermal by their material properties alone. However, we have seen that the chalcogenide materials exhibit athermal advantages of varying degrees compared to Ge, ZnSe and ZnS. If further athermalization is needed, the chalcogenides also have a distinct advantage in reducing the amount of mechanical movement and size necessary to provide passive mechanical compensation. However, material athermalization must also be balanced with manufacturability, as some chalcogenide compositions are more easily processed than others. These processing factors must be taken together with thermal considerations for a balanced solution to each unique application.

When considering that chalcogenide materials are relatively inexpensive, have varied compositions for fine-tuned performance, and benefit from well-established processes that scale to high-volume production, it is clear that they are an excellent choice for thermal lenses. Thorough optical and optomechanical design rigor combined with chalcogenide material options will result in an optimal solution for low-cost and small-size thermal optics.

## ACKNOWLEDGEMENTS

The authors of this paper would like to thank the Infrared Development team at LightPath Technologies for their contributions to this paper. All figures courtesy of LightPath Technologies Inc.

## REFERENCES

[1] Cogburn, G., Mertus, L., Symmons, A., "Molding aspheric lenses for low-cost production versus diamond turned lenses" in *Infrared Technology and Applications XXXVI*, edited by Bjørn F. Andresen, Gabor F. Fulop, Paul R. Norton, Proceedings of SPIE Vol. 7660 (SPIE, Bellingham, WA 2010) 766020.
[2] Bigwood, C., Wood, A., "Two-element lenses for military applications", Opt. Eng. 50 (12), 121705, (2011).
[3] Jamieson, T. H., "Athermalization of optical instruments from the optomechanical viewpoint," Optomechanical Design, Critical Review Vol. CR43, 131-159 (1992).
[4] Schuster, N., Franks, J., "Passive Athermalization of two-lens-designs in 8-12micron waveband", Proc. of SPIE 8353, 835325, (2012).
[5] Grey, D. S., "Athermalization of optical systems," J. Opt. Soc. Am. 38(6), pp. 542-546, (1948).
[6] Povey, V., "Athermalisation Techniques in Infra Red Systems", Proc. SPIE 0655, Optical System Design, Analysis, Production for Advanced Technology Systems, pp. 142-153, (1986).
[7] Tamagawa, Y., Tajime, T., "Expansion of an athermal chart into a multilens system with thick lenses spaced apart", Opt. Eng. 35(10), pp. 3001-3006 (1996).
[8] Riedl, M.J., Optical design fundamentals for infrared systems, Second Edition, SPIE Press, pp.82, 131-133, 2001.
[9] Rayces, J., Lebich, L., "Thermal Compensation of Infrared Achromatic Objectives with Three Optical Materials", SPIE 1354, pp.752-759, (1990).
[10] Schwertz, K., Bublitz, A., Sparrold, S., "Advantages of using engineered chalcogenide glass for color corrected, passively athermalized LWIR imaging systems", Proc. of SPIE 8353, 835326, (2012).
[11] Gleason, B., Wachtel, P., Musgraves, J. D., Qiao, A., Anheier, N., Richardson, K., "Compositional-tailoring of optical properties in IR transparent chalcogenide glasses for precision glass molding", Proc. Of SPIE 8884, 888417, (2013).
[12] Choi, J., Cha, D. H., Kang, H. Y., Kim, J., Kim, H., "Development of chalcogenide glass with thermal stability for molded infrared lens", Proc. SPIE 8982, 89821U, (2014).